Defect Interactions in Anisotropic Two-Dimensional Fluids

R. Stannarius and K. Harth
Institute for Experimental Physics, Otto von Guericke University, D-39106 Magdeburg, Germany
(Received 30 May 2016; published 5 October 2016)

Disclinations in liquid crystals bear striking analogies to defect structures in a wide variety of physical systems, and their straightforward optical observability makes them excellent models to study fundamental properties of defect interactions. We employ freely suspended smectic-*C* films, which behave as quasi-two-dimensional polar nematics. A procedure to capture high-strength disclinations in localized spots is introduced. These disclinations are released in a controlled way, and the motion of the mutually repelling topological charges with strength +1 is studied quantitatively. We demonstrate that the classical models, which employ elastic one-constant approximation, fail to describe their dynamics correctly. In realistic liquid crystals, even small differences between splay and bend constants lead to the selection of pure splay or pure bend +1 defects. For those, the models work only in very special configurations. In general, additional director walls are involved which reinforce the repulsive interactions substantially.

DOI: 10.1103/PhysRevLett.117.157801

Topological defects are found in a broad variety of dynamic physical systems such as anisotropic fluids [1–6], colloids [6–12], superfluid liquids [13,14], quantum systems [15,16], or even in cosmology [17–20]. Similarities between these structures have been pointed out (e.g., Refs. [1,2,20,21]). Defect dynamics are of crucial importance, particularly at phase transitions [22–26]. In cosmology, their direct experimental access is practically impossible. In other systems, one can obtain only indirect experimental evidence [13,14]. Liquid crystals (LCs), however, allow straightforward optical observations, with sample dimensions and time scales in conveniently accessible ranges. First studies of nematic disclinations in the context of understanding primordial cosmological structures were reported by Chuang and co-workers [1,27–29].

Apart from this general interest in LC defects, there are practical aspects. Disclinations mediate forces between colloidal inclusions, being responsible for the self-organization of nematic [4–6] and smectic [30–35] emulsions. Potential applications are, e.g., the preparation of optical vortices [36] or particle trapping [37–39].

Mutual interactions of defects govern the coarsening of Schlieren textures [40–42]: Defect pairs with opposite topological charges attract each other and annihilate. Experiments [3,43–47] and theoretical studies [3,48–53] were performed to understand this elementary coarsening step. One remarkable result was the observation that the defect motion in a pair is asymmetric [45].

Studies in nematics are not easy to interpret because of the three-dimensionality of the problem. Anchoring of the director partially screens defect interactions [47]. The geometry is substantially simpler in a quasi-2D freely suspended film. Nematic (*N*) films are not stable, but stable thin films of tilted smectic-*C* (Sm-*C*) phases can be prepared. Such films can be treated as equivalent to polar nematics in 2D. The azimuthal orientation of the director defines the *c* director, one of the order parameters of the Sm-*C* phase. A pioneering theoretical analysis by Pleiner [54] described friction forces and Brownian motion of disclinations in such films; Svensek [55] and Radzihovsky [56] analyzed particular aspects of the defect dynamics.

Irrespective of the apparent simplicity of the experimental realization, no experimental results have been published to test the theoretical models. This may be due to problems with the preparation of isolated defect pairs in a reproducible way. We introduce a method to create high-strength topological charges in localized traps in Sm-*C* films. They can be released deliberately, to disintegrate into single defects. We follow their trajectories and extract their velocities to test existing models, and demonstrate that important corrections are necessary.

The interaction between two nematic disclinations was calculated by Dafermos [57] under the simplifying assumption of equal splay and bend elastic constants $K_B = K_S = K$ and absence of flow. We may restrict here to disclinations with topological charges ± 1. The force between two such defects separated by a distance r, and acting along the separation vector, is [57,58]

$$f_1 = \pm 2\pi K/r; \tag{1}$$

plus and minus stand for opposite and equal charges, respectively. Within this classical model, interactions of point defects in Sm-*C* films are similar to those of line charges in electrostatics [59]. This result is obtained by superposition of the equilibrium solutions for single defects. It can be applied for multiple defects, too. Then, the net forces are also found by superposition of forces between defect pairs [57]. We will discuss the limits of this model below. As the above authors, we treat the films within an *XY* model. The drag force for ± 1 defects moving with velocity v (with neglect of material flow) was derived as [58]

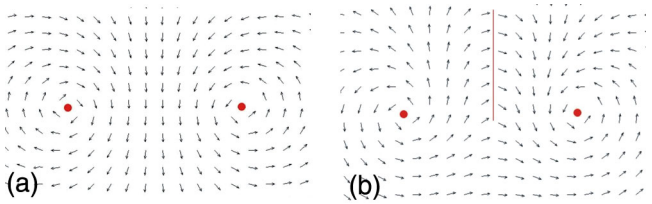

FIG. 1. Sketches of $+1$ defect arrangements (a) $+1R$, $+1L$ pair and (b) two $+1L$ and a superimposed π wall. Only (a) can be achieved by superposition of only two single defects. The red line indicates the ridge of a c-director wall. Other typical configurations are found in the SM [62].

$$f_{\mathrm{drag}} = 2\pi\gamma v \ln(3.6/\mathrm{Er}) \tag{2}$$

with the Ericksen number $\mathrm{Er} = \gamma v r_c/K$ and the defect core radius r_c. In this overdamped system, defect velocities v are given by the balance of f_1 and f_{drag}

$$v = \pm\frac{K}{\gamma \ln(3.6/\mathrm{Er})}\frac{1}{r} = \frac{D_1}{r}. \tag{3}$$

Disregarding the logarithmic v dependence of D_1, one has roughly $|v| \propto r^{-1}$. Again, different signs apply for equal and opposite topological charges, respectively.

This calculation has the beauty that it is analytical and simple. On the other hand, there are three major problems when this model is applied to realistic LC samples: Radzihovsky [56] recently noted that defect motion alters the surrounding c-director field. Corrections of the interaction potentials are needed depending on the relations between defect core size r_c, separation r, and some velocity-dependent characteristic length (in our experiments of the order of 10 μm). The second problem is the neglect of flow, as shown in numerical simulations [55]: The nonuniform c-director reorientation causes material flow, which in turn influences the c-director dynamics. This is a common feature in nematic and in Sm-C films [60,61]. The flow speeds up the motion of the $+1$ defect in a pair, so that the center of mass of the pair is not conserved [45,51].

There is a third problem, evident in our experiments: The above results are valid only for very special defect configurations. In practice, we consider only three types: Tangential defects of strength $s = +1$ are described by $\theta = \varphi \pm \pi/2$, where φ is the azimuthal angle of the positional vector, with the defect center as the origin of the coordinate system, and θ is the c-director azimuth. The signs $+$ and $-$ of the phase angle define clockwise ($+1R$) or anticlockwise ($+1L$) rotation senses of the c director, respectively (Fig. 1). Another type, the hyperbolic defect of strength $s = -1$, is given by $\theta = \theta_0 - \varphi$, where θ_0 defines an orientation; see the Supplemental Material (SM) [62]. For completeness, we note that $\theta = \varphi$ describes radial $+1$ defects. Practically all Sm-C materials have different elastic constants for splay and bend $K_S \neq K_B$. If the difference is not too large, solutions of the Laplace equation for θ may still be reasonable approximations for the c director far from defects, but in the vicinity of $+1$ defect cores, where the elastic energy density diverges, the material always chooses the deformation with the lower elastic constant [63]. In nonpolar Sm-C, this is typically K_B, and all $+1$ defects are tangential [64]. For the material studied here, $K_S \approx 2.2K_B$ (see the Supplemental Material [62]).

This has several important consequences. First, in a $(+1,-1)$ defect pair, one needs to consider the orientation θ_0 of the -1 defect relative to the $+1$ defect. In general, elastic forces will rotate the -1 defect and distort the trajectories which are no longer straight paths towards the opponent. But, even if one has only $+1$ defects, problems arise: Between two neighboring $+1L$ (or two $+1R$) defects [Fig. 1(b)], there has to be an inversion wall which changes their interaction potential. For more than two $+1$ defects, the issue of frustration adds intricacy: One can have a wall-free ($+1R$, $+1L$) defect pair described by Eq. (1), but if a third tangential $+1$ defect is added, intermediate walls of the c director have to be introduced, in general (see the SM [62]). Because any such wall repels the neighboring defects, the interactions are much more complex than described with the simple one-constant model in Eq. (1) (where the phase angle is freely adjustable). The bottom line is that in our simple experiments reported below, defect interactions will be *qualitatively different* from those predicted by all earlier models. The corrections introduced for flow fields [55] and structure corrections in moving defects [56] are negligible with respect to the influences of inversion walls, as soon as $K_B \neq K_S$, which is practically always the case.

We study a nonchiral room-temperature Sm-C binary (50 vol%:50 vol%) mixture of 5-n-Octyl-2-[4-(n-Octyloxy) phenyl]pyrimidine and 5-n-Octyl-2-[4-(n-Hexyloxy)phenyl] pyrimidine, phase sequence Sm-C $\overline{45\text{–}47\,^{\circ}\mathrm{C}}$ Sm-A $\overline{60.6\,^{\circ}\mathrm{C}}$ N $\overline{66\,^{\circ}\mathrm{C}}$ Iso. In one experiment (the $S = 2$ defect pair), a 50:50 mixture of the homologues 5-n-Octyl-2-[4-(n-Hexyloxy)phenyl]pyrimidine and 5-n-Decyl-2-[4-(n-Octyloxy)phenyl]pyrimidine was used, phase sequence Sm-C $\overline{52\,^{\circ}\mathrm{C}}$ Sm-A $\overline{68\,^{\circ}\mathrm{C}}$ N $\overline{72\,^{\circ}\mathrm{C}}$ Iso.

Films with thicknesses of the order of 1 μm are drawn over a rectangular frame of about 4 mm width. Their width can be manipulated by moving one of the edges; thereby, the film area can be rapidly changed. For temperature control and shielding from air flow, the samples are placed in a Linkam THMS400 hot stage. The measurements are performed at room temperature with a Carl Zeiss Axio Imager for Polarized Light Microscopy, Axio cam HR camera, and AxioVision software; frame rates of the videos are between 5 and 30 frames per second.

The c-director field in the film is extracted from transmission images under crossed polarizers, in most experiments with a diagonally inserted λ phase plate (550 nm, slow axis from top right to bottom left). Then, locations where the c director is diagonal to the analyzer appear bluish (/) or reddish (\); see the SM for details [62].

For the preparation of high-strength disclinations, we need inhomogeneous director fields. Stripe textures carrying point disclinations at their tips were found to expand spontaneously from the meniscus into uniform film regions [65–67]. We prepare them in a controlled way. The film

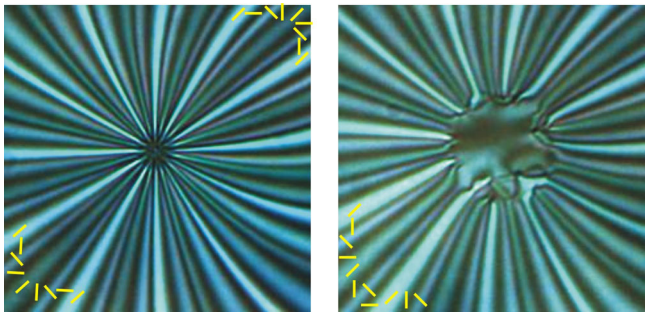

FIG. 2. Twelve defects trapped in a hole in equilibrium (left) and the same hole after expansion of the film area (right), whereby the hole grows in size. Crossed polarizers (+), no phase plate, image dimensions 72 μm × 72 μm. Yellow lines sketch the c director; the sense of direction cannot be distinguished from these images.

width is slowly reduced until the opposing menisci get in contact. Then, the film width is carefully increased in order to stabilize a small thinner region in an otherwise thick, homogeneous film area. Layer steps around that hole trap defects that remain bound to thinner film regions for energetic reasons, as seen in Fig. 2. Then, the competing elastic and capillary forces create an equilibrium structure with the total topological strengths S of all trapped defects (in our experiments, up to 15 defects of charge +1). Capillary forces and the dislocations surrounding the hole pull inwards, the defects push outwards, and equilibrium hole sizes are of the order of a few μm.

Then, the film area can be expanded arbitrarily, while the high-strength defect structure remains trapped. When the total film area is quickly reduced afterwards by a few percent, the hole can be deliberately eliminated. Thereafter, the trapped +1 disclinations discharge and their trajectories can be used to determine interaction potentials. Often, symmetric arrangements are observed, with one defect remaining in the center. A typical example is shown in Fig. 3 for $S = 9$. We cannot extract the actual sign of the c director with our setup optically, but when we assign a direction sense in any spot of the image, all other directions are fixed. We will assign one defect in an image arbitrarily as $+1R$; then, all others are fixed. With the opposite assignment, the results would be identical. The peripheral +1 defects in Fig. 3 all have the same direction sense (L), opposite to the central one (R). Thus, inversion walls must separate all neighboring peripheral defects. This is clearly evident in the image. The details of the c-director field extracted from the images can be found in the SM [62].

After release of the defect cloud, we measure the positions of all defects. In good approximation, all configurations expand self-similarly when all spatial distances are rescaled $\propto t^{1/2}$, neglecting the slight v dependence in the logarithm in Eq. (2). This is a consequence of the nematodynamic equations which contain only terms with second spatial derivatives and first time derivatives, provided that the structures are much larger than defect cores

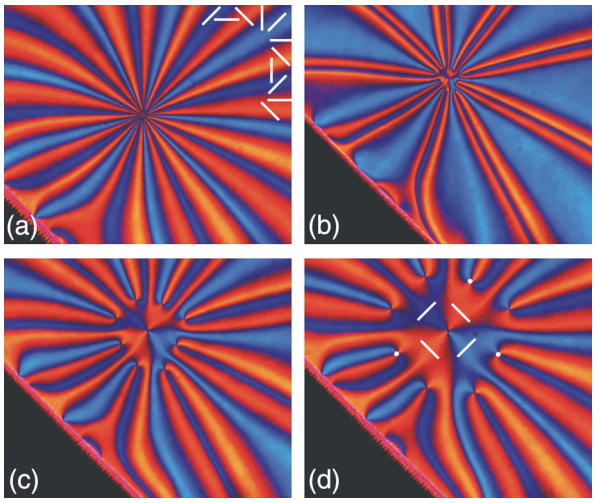

FIG. 3. (a) Nine trapped defects in a hole of approximately 10 μm diameter. (b) Exploding configuration immediately after the hole has been extinguished by pushing the barrier (left bottom corner) inward. The narrowed brushes indicate transient flow alignment of the c director. Single defects (c) 1.8 s after release and (d) 5 s after release. Dimensions are 475 μm × 400 μm. For an explanation of the white dots, see the text.

and film boundary influences are negligible. A more complex example is seen in Fig. 6 below.

If one extends the classical model [Eq. (1)] to arrangements with one +1 defect in the center and $(S-1)$ defects arranged symmetrically on a circle with radius r moving out radially, then a superposition of forces with neglect of inversion walls gives $f_S = Sf_1/2$. Each symmetric pair of defects on the hypothetical regular $(S-1)$ polygon contributes a force $2f_1/2$ (see the inset of Fig. 4). Figure 4 shows the experimental data in log-log scale. There is good agreement with a square-root law $r = (2Dt)^{1/2}$ resulting from $v = D/r$. The data for the $S = 9$ configuration of Fig. 3 and a symmetric $S = 7$ configuration with a central defect at rest and the outer defects in a regular hexagon are included.

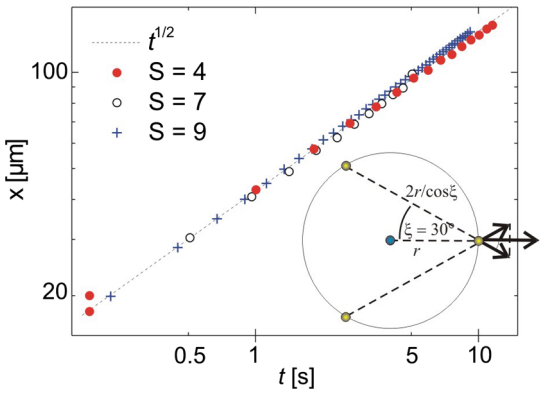

FIG. 4. Displacement as a function of time for the three peripheral defects in an $S = 4$ configuration, the eight outer defects of Fig. 3 ($S = 9$), and six outer defects of a symmetric $S = 7$ configuration. The inset shows the forces in the classical model; only the radial components add up, and the tangential ones compensate each other.

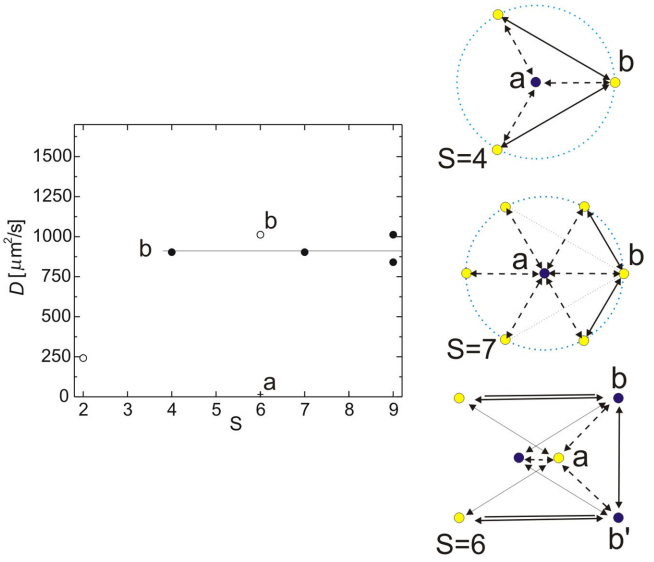

FIG. 5. Scaling factor $D = vr$ for symmetric configurations (solid circles) with one central and $S - 1$ peripheral defects; open circles show $S = 2$, and $S = 6$ where two inner defects and four peripheral defects appear. The solid line is an average of the D values extracted for peripheral defects of the $S = 4$, 7, and 9 configurations. Typical configurations and forces are sketched in three graphs (see the text). Colored dots distinguish the R and L defects.

Within experimental accuracy, they coincide with the $S = 4$ dynamics, which is convincing evidence that the classical model is inappropriate. Within that model, the scaling parameters $D = vr$ should relate like 4:7:9 for the respective configurations. Figure 5 combines the scaling factors D for defects in several configurations. In the $S = 4$ and $S = 7$ cases shown, all outer defects move with the same velocity. In the $S = 9$ structure, three defects (marked by white dots in Fig. 3) move 15% slower than the other five. The proximity of the lateral film edge (bottom left of the image) is evidently not the cause of a measurably slower defect speed, even though the c director is planarly anchored there.

Assuming that the *drag force* on individual defects is hardly influenced by the other defects, we attribute the different D to differences in the interaction forces, so we need to add corrections to Eq. (1). A closer look at the defect environments reveals that one deals with very different types of interactions. They are sketched in Fig. 5. For better clarity, only forces to the labeled defects are shown; the others are found from symmetry. Neighboring defects with opposite handedness experience a mutual force f_1 (thick dashed lines), where $D_1 \approx 250\ \mu\text{m}^2/\text{s}$ can be estimated from the $S = 2$ case. Neighboring defects of same handedness with an intermediate π wall experience a larger force $f_w > f_1$ (thick solid lines) because of the additional elastic forces of the wall; double lines indicate 2π walls. From the $S = 4$ case, one can estimate this to contribute an additional $D_w \approx 665\ \mu\text{m}^2/\text{s}$. Any defect located between a pair screens their interactions (thin lines) partially or completely. The reason for that is obvious: At the intermediary defect, the director field is fixed to tangential anchoring, so a direct influence of the two defects on opposite sites on each other is inhibited, at least partially. Therefore, the far away located defects have only little influence on a given defect; this explains why $S = 9$ and $S = 7$ are practically equivalent to $S = 4$. The effectiveness of this shielding depends upon the defect positions and is difficult to calculate quantitatively.

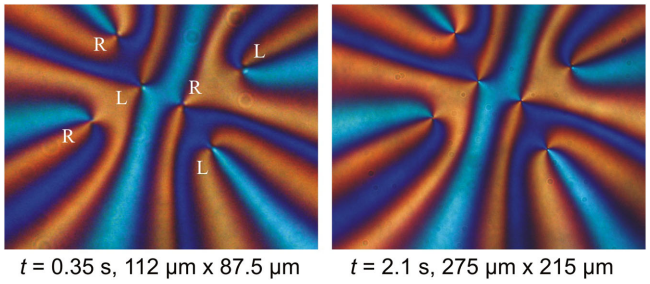

FIG. 6. Two snapshots of an $S = 6$ configuration after release, with two inner defects and four outer defects; all spatial distances scale with the square root of time. R and L mark the directional senses.

More complex configurations may have two inner defects, as shown exemplarily for an $S = 6$ configuration in Fig. 6; they also scale self-similarly. Such more complex arrangements (see also $S = 8$ shown in the SM [62]) need a numerical treatment of the force balances.

Summarizing, we have introduced a preparation technique for high-strength defect structures in smectic-C films and employed it to study defect dynamics. The experimental data reveal the limitations of the classical defect interaction models in liquid crystals. Important corrections are required in all practical situations. Director walls need to be introduced; their presence dominates the relaxation. The frustration of multiple +1 defect configurations is obvious for the polar c director, but similar problems exist in nonpolar nematic liquid crystals when the elastic anisotropy enforces exclusively tangential (or radial) +1 defects: It is impossible to construct a director field of three such +1 defects without having to add director walls or additional point defects (see the SM [62]). Therefore, considerable qualitative corrections are essential in any coarsening scenarios even in nematics, when $K_S \neq K_B$.

We thank Peter Salamon and Alexey Eremin for contributions to the experiments. Financial support by the Deutsche Forschungsgemeinschaft (Project No. STA 425/28), by the Deutsches Zentrum für Luft- und Raumfahrt (Project No. 50WM1430), and the Deutscher Akademischer Austauschdienst/MÖB (Grant No. 64975) is acknowledged.

[1] I. Chuang, R. Durrer, N. Turok, and B. Yurke, Science **251**, 1336 (1991).
[2] M. J. Bowick, L. Chandar, E. A. Schiff, and A. M. Srivastava, Science **263**, 943 (1994).
[3] M. Kleman and O. D. Lavrentovich, Philos. Mag. **86**, 4117 (2006).
[4] T. C. Lubensky, D. Pettey, N. Currier, and H. Stark, Phys. Rev. E **57**, 610 (1998).

[5] H. Stark, Phys. Rep. **351**, 387 (2001).
[6] P. Poulin, H. Stark, T. C. Lubensky, and D. A. Weitz, Science **275**, 1770 (1997); P. Poulin and D. A. Weitz, Phys. Rev. E **57**, 626 (1998).
[7] I. Musevic, M. Skarabot, U. Tkalec, M. Ravnik, and S. Žumer, Science **313**, 954 (2006).
[8] U. Tkalec, M. Ravnik, S. Copar, S. Žumer, and I. Musevic, Science **333**, 62 (2011).
[9] W. T. M. Irvine, V. Vitelli, and P. M. Chaikin, Nature (London) **468**, 947 (2010).
[10] U. Gasser, C. Eisenmann, G. Maret, and P. Keim, ChemPhysChem **11**, 963 (2010).
[11] W. T. M. Irvine, A. D. Hollingsworth, D. G. Grier, and P. M. Chaikin, Proc. Natl. Acad. Sci. U.S.A. **110**, 15544 (2013).
[12] A. Libál, C. Reichhardt, and C. J. Olson Reichhardt, Phys. Rev. E **75**, 011403 (2007).
[13] C. Bäuerle, Yu. M. Bunkov, S. N. Fisher, H. Godfrin, and G. R. Picket, Nature (London) **382**, 332 (1996).
[14] V. M. H. Ruutu, V. B. Eltsov, A. J. Gill, T. W. B. Kibble, M. Krusius, Yu. G. Makhlin, B. Plaçais, G. E. Volovik, and W. Xu, Nature (London) **382**, 334 (1996).
[15] A. Polkovnikov, K. Sengupta, A. Silva, and M. Vengalattore, Rev. Mod. Phys. **83**, 863 (2011).
[16] C. N. Weiler, T. W. Neely, D. R. Scherer, A. S. Bradley, M. J. Davis, and B. P. Anderson, Nature (London) **455**, 948 (2008).
[17] T. W. B. Kibble, J. Phys. A **9**, 1387 (1976).
[18] W. H. Zurek, Nature (London) **317**, 505 (1985).
[19] M. B. Hindmarsh and T. W. B. Kibble, Rep. Prog. Phys. **58**, 477 (1995).
[20] W. H. Zurek, Phys. Rep. **276**, 177 (1996).
[21] T. Kibble and A. Srivastava, J. Phys. Condens. Matter **25**, 400301 (2013) and the following Special Section on Condensed Matter Analogues of Cosmology of that volume.
[22] A. M. Bibo and I. R. Peterson, Thin Solid Films **210–211**, 515 (1992).
[23] A. J. Bray, Adv. Phys. **43**, 357 (1994).
[24] B. Damski, Phys. Rev. Lett. **95**, 035701 (2005).
[25] V. B. Eltsov, R. Hänninen, and M. Krusius, Physica (Amsterdam) **470C**, 803 (2010).
[26] Y.-K. Kim, S. V Shiyanovskii, and O. D Lavrentovich, J. Phys. Condens. Matter **25**, 404202 (2013).
[27] I. Chuang, N. Turok, and B. Yurke, Phys. Rev. Lett. **66**, 2472 (1991).
[28] B. Yurke, A. N. Pargellis, I. Chuang, and N. Turok, Physica (Amsterdam) **178B**, 56 (1992).
[29] I. Chuang, B. Yurke, A. N. Pargellis, and N. Turok, Phys. Rev. E **47**, 3343 (1993).
[30] R. Najjar and Y. Galerne, Mol. Cryst. Liq. Cryst. **367**, 475 (2001).
[31] P. Cluzeau, G. Joly, H. T. Nguyen, and V. K. Dolganov, JETP Lett. **75**, 482 (2002).
[32] P. Cluzeau, G. Joly, H. T. Nguyen, and V. K. Dolganov, JETP Lett. **76**, 351 (2002).
[33] P. Cluzeau, V. Bonnand, G. Joly, V. Dolganov, and H. T. Nguyen, Eur. Phys. J. E **10**, 231 (2003).
[34] C. Völtz and R. Stannarius, Phys. Rev. E **70**, 061702 (2004).
[35] C. Völtz and R. Stannarius, Phys. Rev. E **72**, 011705 (2005).
[36] S. Fumeron, E. Pereira, and F. Moraes, Physica (Amsterdam) **476B**, 19 (2015).
[37] J.-B. Fleury, D. Pires, and Y. Galerne, Phys. Rev. Lett. **103**, 267801 (2009).
[38] D. Coursault, J. Grand, B. Zappone, H. Ayeb, G. Lvi, N. Félidj, and E. Lacaze, Adv. Mater. **24**, 1461 (2012).
[39] D. Coursault *et al.*, Soft Matter **12**, 678 (2016).
[40] B. Yurke, A. N. Pargellis, T. Kovacs, and D. A. Huse, Phys. Rev. E **47**, 1525 (1993).
[41] S. Digal, R. Ray, P. S. Saumia, and A. M. Srivastava, J. Phys. Condens. Matter **25**, 404204 (2013).
[42] R. Repnik, A. Ranjkesh, V. Simonka, M. Ambrozic, Z. Bradac, and S. Kralj, J. Phys. Condens. Matter **25**, 404201 (2013).
[43] H. V. Ribeiro, R. R. Guimarães, R. T. Teixeira-Souza, H. Mukai, P. R. G. Fernandes, E. K. Lenzi, and R. S. Mendes, Phys. Rev. E **87**, 054501 (2013).
[44] R. R. Guimarães, R. S. Mendes, P. R. G. Fernandes, and H. Mukai, J. Phys. Condens. Matter **25**, 404203 (2013).
[45] P. Oswald and J. Ignes-Mullol, Phys. Rev. Lett. **95**, 027801 (2005).
[46] I. Dierking, M. Ravnik, E. Lark, J. Healey, G. P. Alexander, and J. M. Yeomans, Phys. Rev. E **85**, 021703 (2012).
[47] A. Bogi, P. Martinot-Lagarde, I. Dozov, and M. Nobili, Phys. Rev. Lett. **89**, 225501 (2002).
[48] M. Reichenstein, H. Stark, J. Stelzer, and H.-R. Trebin, Phys. Rev. E **65**, 011709 (2001).
[49] G. Tóth, C. Denniston, and J. M. Yeomans, Phys. Rev. Lett. **88**, 105504 (2002).
[50] A. M. Sonnet and E. G. Virga, Liq. Cryst. **36**, 1185 (2009).
[51] D. Svenšek and S. Žumer, Phys. Rev. E **66**, 021712 (2002).
[52] D. Svenšek and S. Žumer, Phys. Rev. E **70**, 061707 (2004).
[53] C. D. Muzny and N. A. Clark, Phys. Rev. Lett. **68**, 804 (1992).
[54] H. Pleiner, Phys. Rev. A **37**, 3986 (1988).
[55] D. Svensek and S. Zumer, Phys. Rev. Lett. **90**, 155501 (2003); D. Svensek and S. Zumer, Phys. Rev. Lett. **90**, 219901(E) (2003).
[56] L. Radzihovsky, Phys. Rev. Lett. **115**, 247801 (2015).
[57] C. M. Dafermos, Q. J. Mech. Appl. Math. **23**, 49 (1970).
[58] M. Kleman and O. D. Lavrentovich, *Soft Matter Physics: An Introduction* (Springer Verlag, New York, 2003).
[59] W. G. Jang, V. V. Ginzburg, C. D. Muzny, and N. A. Clark, Phys. Rev. E **51**, 411 (1995).
[60] K. Harth, A. Eremin, and R. Stannarius, Soft Matter **7**, 2858 (2011).
[61] R. Stannarius, C. Bohley, and A. Eremin, Phys. Rev. Lett. **97**, 097802 (2006).
[62] See Supplemental Material at http://link.aps.org/supplemental/10.1103/PhysRevLett.117.157801 for more qualitative examples of director fields around defect configurations, for a more detailed description of the relation between the director fields and optical textures, for the derivation of the elastic constants ratio from the observed textures, and for a discussion of multiple defects in ordinary (non-polar) nematics.
[63] A. Eremin, C. Bohley, and R. Stannarius, Phys. Rev. E **74**, 040701(R) (2006).
[64] In polar Sm-*C*, the effective bend elastic constant may be larger than K_S because of electrostatic contributions from polarization splay; then, the +1 defects will be exclusively radial. The effects are nevertheless the same, with two types of defects having the *c* director pointing inward or outward.
[65] J. E. Maclennan, Europhys. Lett. **13**, 435 (1990).
[66] K. Harth and R. Stannarius, Eur. Phys. J. E **28**, 265 (2009).
[67] K. Harth, A. Eremin, and R. Stannarius, Ferroelectrics **431**, 59 (2012).